ADVANCED INTELLIGENT SYSTEMS
Open Access
www.advintellsyst.com

An Electric Self-Sensing and Variable-Stiffness Artificial Muscle

*Chen Liu, James J. C. Busfield, and Ketao Zhang**

Soft robots have better flexibility than their rigid counterparts thus offering greater adaptability to changing environments. These robots made from flexible materials are generally with low stiffness and have limited capability to perform tasks that require the application of large forces. Soft artificial muscles (AMs) with variable stiffness are promising solutions for soft robots to handle larger payloads. However, the existing actuators need to overcome their small range of stiffness variation and slow response. Further, it is difficult to integrate self-sensing into existing actuators. Herein, a novel electric AM with variable stiffness and self-sensing referencing smooth muscle contraction in nature is proposed. The AM consists of two pieces of soft anode mesh, a flexible cathode and a polyvinyl chloride (PVC) gel dielectric layer, where the cathode is also a resistive sensor. The stiffness variation is induced by the friction change caused by electrostatic adsorption. Compared with the existing PVC gel actuation technology, the new design integrated the dielectric and the cathode layers and combined the sensing function. Also, the rigid anode and cathode are replaced by the soft ones, respectively, which makes the AM suitable for soft robotics or wearable devices.

1. Introduction

Recent advances in artificial muscles (AMs) with variable stiffness[1–3] have greatly contributed to the extensive development of bionic and soft robotics.[4,5] The combination of variable stiffness and flexibility enables these robots to adapt to complex and changing environments and to perform multiple tasks in comparison with traditional rigid-bodied[6,7] or fully soft robots.[8–11] For instance, a soft gripper with stiffness variation is able to provide a sufficient grip while not damaging fragile objects.[12] In addition, soft robots use inherent compliance to get through tight spaces but can still increase their load-bearing capacity by increasing their stiffness.[13,14] According to the energy supply, soft robots with stiffness variation can be classified into three types: 1) the pneumatic variable-stiffness designs, typically utilizing the form of jamming structures, have excellent stiffness adjustment (at least ten times) and rapid rate (under 1 s) but requires a bulky air source and a range of pneumatic circuitry.[15,16] 2) The thermodynamic variable-stiffness designs typically adopt shape memory alloy[17] or low-melting-point alloy[18] configurations, achieve variable stiffness primarily through the phase change of the materials, and are effective for applications whose stiffness can be modified through temperature change of environments. However, the response speed (generally over 1 s) needs further improvement.[19,20] 3) Electric variable-stiffness designs have been proposed in recent years to provide new solutions based on electrostatic adsorption technology. Robots that adopt these designs have an extremely fast response rate (under 100 ms) and can be controlled by electricity directly.[21–24] In addition to the stiffness variation, the operation of robots also relies on sensing, which gives them feedback on motion and forces, which improves their ability to adapt to the environment.[25,26] In particular, compared with traditional rigid sensors, flexible sensors have better compliance and fit soft robots seamlessly.[27–30]

In recent years, the emergence of self-sensing variable-stiffness (SSVS) AMs has provided new ideas for the development of robots.[31] The designs that integrated actuation with variable stiffness and sensing have significantly simplified the robot construction[32,33] and represent a step change in the development of soft robots. It envisaged that developing variable-stiffness AMs embedded with sensing functions can dynamically detect deformation and forces, and thus selectively adjust the stiffness.[34–37] For instance, a wearable robot can monitor a patient's activities[38,39] and provide resistance by applying different stiffnesses, which will help restore muscle function during rehabilitation training.[40,41]

The polyvinyl chloride (PVC) gel electric actuation technology is an existing smart actuation technology. The working principle is that the electrostatic force produced by the high voltage on the anode attracts PVC gel into the mesh, causing the structure to become thinner, so as to achieve the driving effect.[42,43] In previous studies, the PVC gel actuation technology is mainly applied to the actuation of soft robots. AMs based on that integrating

C. Liu, J. J. C. Busfield, K. Zhang
School of Engineering and Materials Science
Queen Mary University of London
London E1 4NS, UK
E-mail: ketao.zhang@qmul.ac.uk

The ORCID identification number(s) for the author(s) of this article can be found under https://doi.org/10.1002/aisy.202300131.

© 2023 The Authors. Advanced Intelligent Systems published by Wiley-VCH GmbH. This is an open access article under the terms of the Creative Commons Attribution License, which permits use, distribution and reproduction in any medium, provided the original work is properly cited.

DOI: 10.1002/aisy.202300131

variable-stiffness technology and sensing function have not yet been proposed.[44] In this article, we propose a new electric SSVS-AM aimed at achieving a significant stiffening effect and capacity of sensing strain and resultant force. By measuring the corresponding stiffnesses at different voltages, the value of the external load can be calculated by detecting the deformation through the sensor. We demonstrate a manufacturing method that guarantees the bond between the sensor and the dielectric films. This leads to a new type of soft-bodied AMs capable of close-loop sensing and actuation, without requirements for assembly of separate sensors and actuators in various forms. The SSVS-AM provides a new solution for the development of soft robots and wearable devices.

2. Results and Discussion

2.1. Design of the SSVS-AM

Smooth muscles become stiffer due to the contraction when they receive stimulation, as shown in **Figure 1**a. The underlying principle of the increase in stiffness is that the intermediate filaments and dense bodies are tightened, so the muscle cells are squeezed, leading to bigger density and thus stiffer body.[45–47] Inspired by that, we propose the SSVS-AM, which consists of three essential elements: 1) the soft fiber metal mesh (with a bending modulus <1 GPa) as the anode, which plays a role as the intermediate filament and the dense body; 2) the PVC gel dielectric layer; and 3) the flexible conductive cathode, as shown in Figure 1a. The PVC gel layer wraps around the cathode layer and they are bonded together with good stretchability, which is defined as the "stretchable layer" and plays the role of the muscle cell in the smooth muscle. Compared to that, although the metal mesh can be bent relatively easily, it is difficult to stretch so it guarantees stiffness in the tensile direction. The variable stiffening working principle is shown in Figure 1b. When the voltage is off, the structure is soft and can be stretched in the longitudinal direction by keeping one end of the metal mesh bonded to the stretchable layer. When the voltage is applied to the structure, the anode attracts the dielectric layer into the mesh due to the effect of electrostatic force, limiting the structure from being stretched. The structure is in a stiffer state, and its stiffness is thus increased. In addition, as for the sensing principle, the cathode layer is a conductive layer with carbon nanotubes (CNT) incorporated into Ecoflex 00-30, which increases in resistance with

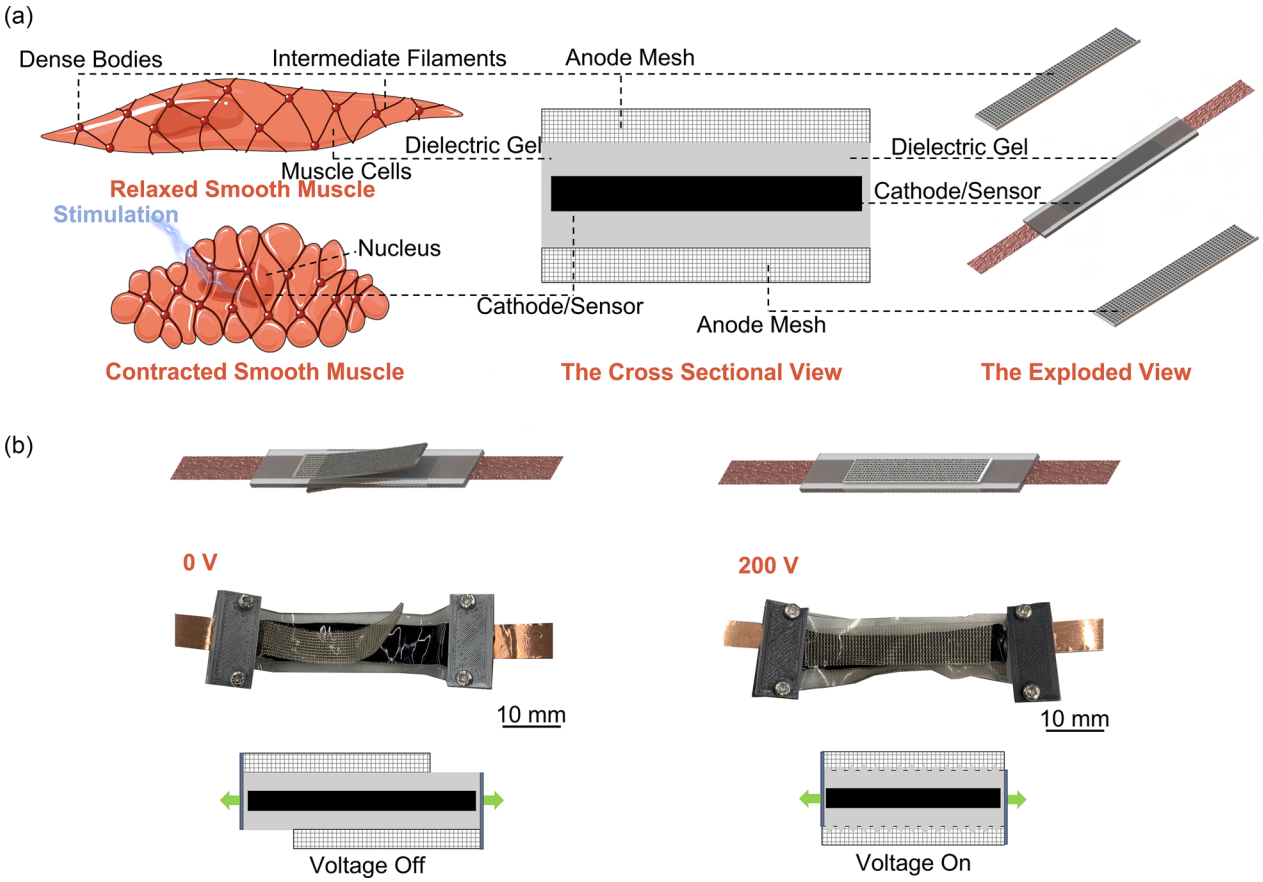

Figure 1. a) The self-sensing variable-stiffness artificial muscle (SSVS-AM) is inspired by the stiffness-increasing process of the smooth muscle,[54] and the schematic shows that the SSVS-AM consists of the soft anode mesh, dielectric gel layer, and flexible cathode, which is also a resistive sensor. b) Without applying voltage on the SSVS-AM, the meshes don't absorb the dielectric gel, and the structure can be stretched easily. Applying a voltage of 200 V on the SSVS-AM, with the effect of the electrostatic field, the meshes absorb the dielectric gel and compress it, and the SSVS-AM becomes harder to be stretched because of the increased friction between meshes and the dielectric gel.

© 2023 The Authors. Advanced Intelligent Systems published by Wiley-VCH GmbH

26404567, 2023, 9, Downloaded from https://advanced.onlinelibrary.wiley.com/doi/10.1002/aisy.202300131 by Head Of Financial Services Bolland Library, Wiley Online Library on [14/10/2025]. See the Terms and Conditions (https://onlinelibrary.wiley.com/terms-and-conditions) on Wiley Online Library for rules of use; OA articles are governed by the applicable Creative Commons License

26404567, 2023, 9, Downloaded from https://advanced.onlinelibrary.wiley.com/doi/10.1002/aisy.202300131 by Head Of Financial Services Bolland Library, Wiley Online Library on [14/10/2025]. See the Terms and Conditions (https://onlinelibrary.wiley.com/terms-and-conditions) on Wiley Online Library for rules of use; OA articles are governed by the applicable Creative Commons License

stretching, making it a resistive sensor. The sensor monitors the length change in real time and the AM can adjust the stiffness in response. Therefore, the SSVS-AM is an intelligent AM that incorporates integrated sensing with variable stiffness.

2.2. Fabrication of the SSVS-AM

A rectangular shape is chosen for tensile testing because it is easy to manufacture and can provide accurate measurement results. In addition, a rectangular shape undergoes uniform strain during tensile testing, which makes the measurement results reliable and precise. Therefore, we design the sample with a rectangular shape as shown in Figure 1b. An electronic cutter (Cricut Maker, Inc. USA) is used to cut anodes with 40–100 mesh and a thickness of 100 μm. PVC gel is obtained by dissolving PVC particles with an average molecular weight of 4400 using dibutyl adipate (DBA) as the plasticizer. To obtain the conductive solution, CNT, Ecoflex 00-30 components A and B are mixed, heated, and stirred to make cross-linking between the components. The preparation of the solutions and the layers is detailed in Supporting Information. The PVC solution and the conductive solution are cast separately on a casting machine. The first PVC gel layer is cast first, the conductive layer is cast after the first PVC gel layer curing, then another PVC gel layer is cast after the conductive layer curing encapsulation. The two PVC gel layers are integrated to wrap the conductive layer as a stretched layer after curing. The three-layer structure thus formed is effectively bonded, as shown in **Figure 2**a, ensuring its stability when used as a sensor. As shown in Figure 2b, the copper tape is used to connect to the conductive layer prior to the PVC gel encapsulation to ensure a low contact resistance value (under 100 Ω). The final step is to fix the two ends of the muscle structure using 3D-printed clamps and screws, as shown in Figure 2c. Each end is fixed to only one mesh to guarantee the other end of the mesh is free.

2.3. Variable Stiffness of the SSVS-AM

To improve the variable-stiffness performance of the SSVS-AM, we explored ways to increase the adsorption effect of the anode on the gel within a limited voltage (700 V). The variables include the dimension of the conductive mesh, the components' mass ratio, and the thickness of the gel.[48] Among them, the components' mass ratio affects the dielectric and mechanical parameters of the gel. The thickness and viscosity of the gel film and the mesh size directly affect the gel filling in the mesh. The working principle of the PVC gel actuator is the creeping deformation of the PVC gel film between the electric fields of the cathode and anode toward the anode grid.[49] It implies that the size of the holes in the anode metal grid has a direct impact on the final shrinkage of the actuator.

The stiffness variation is directly related to the amount of deformation of the PVC gel actuator, where the mesh size of the anode mesh and the physical properties such as the thickness and viscosity of the PVC gel are key effect factors. The mesh index represents the number of holes in a length of 1 inch (approximately 25.41 mm). Porosity ξ is a key indicator. The larger ξ, the larger the volume of PVC gel that can be filled within a fixed anode area, and the better the performance of the SSVS-AM absorber.

In a closed view of the anode mesh shown in **Figure 3**a, in which the mesh index is n, and the diameter of the wire is Φ. A square hole is a unit with a side length of

$$l = 25.41/n \tag{1}$$

The volume of a unit is given by

$$V = 2\Phi l^2 \tag{2}$$

where 2Φ is the thickness.

The volume of the wire is given by

$$V' = \pi\Phi\sqrt{l^2 + \Phi^2} \tag{3}$$

The proportion of pore space in a square pore unit to the total volume (the porosity) is defined as

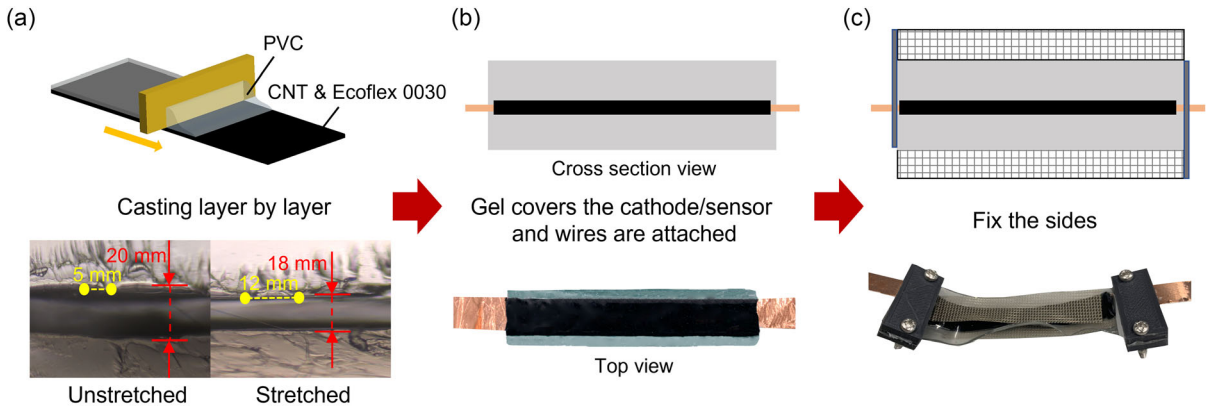

Figure 2. The approximate fabrication process of the SSVS-AM. a) The layer's casting using prepared polyvinyl chloride (PVC) gel solution and conductive solution mixing carbon nanotube (CNT) and Ecoflex 00-30 (the details of the casting process are given in Supporting Information) and the image shows the stable bonding interface between the PVC gel layer and conductive layer when they are stretched up to 140%. b) The copper tape is used to connect the conductive layer and outside power. c) The two sides of the structure are fixed by the 3D-printed panels and screws.

© 2023 The Authors. Advanced Intelligent Systems published by Wiley-VCH GmbH

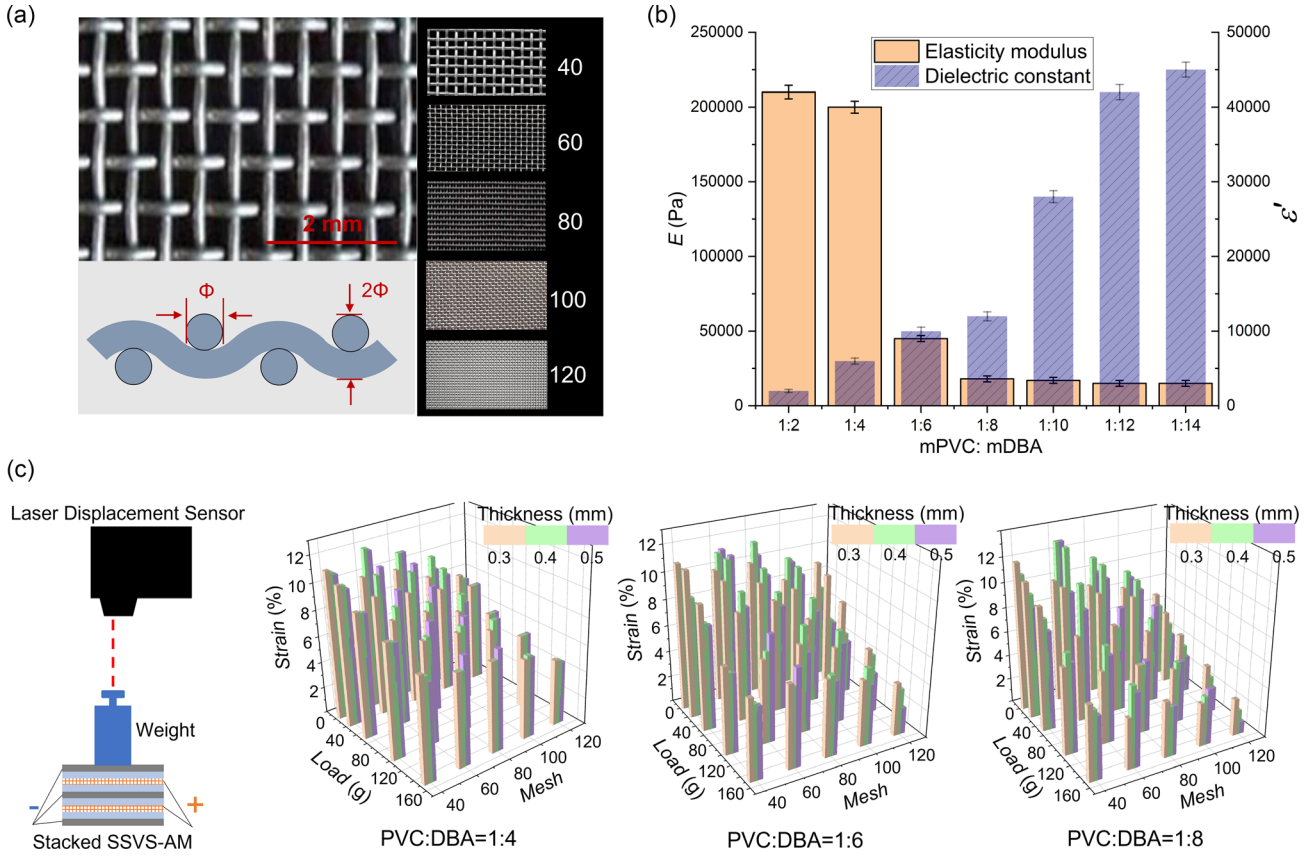

Figure 3. a) The structure and parameters of the mesh and the picture of different meshes used in the experiment. b) The different effects in the elasticity modulus and the dielectric constant of the PVC gel are caused by the changing mass ratios of the components (PVC and dibutyl adipate [DBA]). The ratio and the dielectric constant are positively correlated while the ratio and the elasticity modulus are negatively correlated. c) The multiple combination experiments. The measuring system consists of one laser displacement sensor, weights, and stacked SSVS-AMs with a power supplier. The testing results show the relationship among the components (PVC and DBA) ratios, loads, meshes, strains of the actuation, and the thicknesses of the PVC gel. There is a total of 75 combinations.

$$\xi = 1 - \frac{V'}{V} = 1 - \frac{\pi\Phi}{2}\sqrt{\frac{l^2 + \Phi^2}{l^4}} \tag{4}$$

The ratio of the diameter of the wire mesh to the spacing is given by

$$\alpha = \frac{\Phi}{l} \tag{5}$$

Therefore

$$\xi = 1 - \frac{\pi\alpha}{2}\sqrt{\alpha^2 + 1} \tag{6}$$

As expressed in Equation (6), the porosity is related to the size of the wire. In this work, 40, 60, 80, and 100 mesh flexible conductive meshes (Figure 3a) are selected separately for calculation, and the results are shown in **Table 1**.

The analytical results indicate that a 40 mesh allows the PVC gel to be filled with the maximum volume and shrinkage displacement. However, in practice, the shrinkage displacement of the PVC drive does not only depend on the porosity of the metal mesh but also on the physical parameters of the PVC gel itself. This still needs to be verified by suitable thickness, modulus of elasticity, and viscosity measurements to combine theory with practice.

Table 1. The parameters of each mesh.

Mesh	ϕ/mm	l [mm]	α [NA]	ξ[%]
40	0.20	0.635	0.315	48.1
60	0.15	0.423	0.355	40.8
80	0.12	0.318	0.377	36.7
100	0.10	0.254	0.394	33.5
120	0.08	0.212	0.377	36.7

The components ratios of the PVC gel determine the modulus of elasticity (E) and the dielectric constant (ε'), which determines the ease with which it can be deformed under an electric field. The different ratios of PVC gel materials determine the modulus of elasticity and the dielectric constant of the PVC gel; hence, the ease of deformation under electric fields. As shown in Figure 3b, the modulus of elasticity and the dielectric constant of the PVC film are inversely related to the mass ratio of PVC and DBA. Both

© 2023 The Authors. Advanced Intelligent Systems published by Wiley-VCH GmbH

26404567, 2023, 9, Downloaded from https://advanced.onlinelibrary.wiley.com/doi/10.1002/aisy.202300131 by Head Of Financial Services Bolland Library, Wiley Online Library on [14/10/2025]. See the Terms and Conditions (https://onlinelibrary.wiley.com/terms-and-conditions) on Wiley Online Library for rules of use; OA articles are governed by the applicable Creative Commons License

the modulus of elasticity and the dielectric constant of the PVC film are inversely related to the mass ratio of PVC and DBA. The modulus of elasticity of the PVC film decreases abruptly when the polymer mass fraction of PVC (mPVC) is less than 20% (mPVC: mDBA [the polymer mass fraction of DBA] = 1: 4), while the dielectric constant increases relatively slowly. Theoretically, a PVC film with a small modulus of elasticity and a large dielectric constant will deform more under an electric field, but a smaller modulus of elasticity will also reduce the output force of the actuator. In previous theoretical calculations, it is concluded that the porosity of the anode metal mesh determines how well the PVC gel fills in response to the electric field. In practice, the effective thickness of the PVC film will also play a key role in the amount of shrinkage of the drive. The thickness of PVC gel film needs to be reduced as much as possible to ensure adequate mesh filling and to minimize the overall thickness of the actuator. For that reason, PVC films of 0.3 mm (the minimum thickness of the PVC gel that can be accurately controlled by the casting method, the details are given in the experiment section), 0.4 mm, and 0.5 mm thickness are prepared for comparison with different ratios of PVC solutions. The average molecular weight of the PVC powder is 4400, and mPVC: mDBA = 1:4, 1:6, and 1:8 PVC films are prepared. For the anode materials, 40, 60, 80, 100, and 120 mesh stainless steel meshes are used with different ratios and thicknesses of PVC gel film. To amplify the displacement of the SSVS-AM, a multilayer stacking method is adopted for the measurement. Samples of the SSVS-AM stack actuator consisting of five drive unit layers are prepared. The output of each group of actuator specimens is measured to find the best combination of the relevant parameters. Weights of 0, 20, 50, 100, and 150 g are applied with 800 V applied to the actuator, the strains of the test specimens are shown in Figure 3c.

To optimize the variable stiffness of the SSVS-AM by varying component ratios, thicknesses of the PVC film, and meshes of the anode, three combinations are designed as follows.

Combination 1: when mPVC: mDBA = 1: 4, the 0.4 mm thick PVC film, and 60 mesh anode. The best output performance is obtained by matching the 0.4 mm thick PVC film with the 60 mesh anode. The maximum strain on the SSVS-AM driver is 12.36% without load and 6.05% with a 150 g load.

Combination 2: at mPVC: mDBA = 1: 6, a 0.3 mm thick PVC film with an 80 mesh anode gives the best output performance. This gives a maximum strain of 11.91% without load and 5.25% with a 200 g load.

Combination 3: at mPVC: mDBA = 1: 8, a 0.3 mm thick PVC film with a 60 mesh anode gives the best output performance.

The experiment results show that the best output performance is obtained by matching a 0.3 mm thick PVC film with a 60 mesh anode. The SSVS-AM driver has a maximum strain of 13.13% without load. However, with load applied, the response of the driver is reduced and it is susceptible to electrical breakdown. At mPVC: mDBA = 1: 8, the PVC drive has the highest no-load output displacement of 13%. This is due to the fact that the higher DBA content gives the PVC gel a lower modulus of elasticity and a higher dielectric constant, which makes it susceptible to creep deformation under the electric field. However, due to the lower modulus of elasticity, the load-carrying capacity of the drive is reduced and the output displacement is reduced when a higher load is applied.

In addition, the lower modulus of elasticity reduces the load-bearing capacity of the drive, and when a higher load is applied, the output displacement of the drive decreases significantly and is prone to electrical breakdown. The DBA content of the PVC gel needs to be reduced so that the PVC gel actuator can be operated stably. According to the theoretical analysis, the DBA content in the PVC gel needs to be reduced to achieve stable operation. The experimental results show that the output forces and strains of the actuators are good when the 60 mesh is combined with an mPVC: mDBA = 1: 4, the PVC film of 0.4 mm thickness. Therefore, Combination 1 is investigated in this work.

With the selected Combination 1, the stiffness variation of the SSVS-AM is tested. **Figure 4**a illustrates the effect of the SSVS-AM with and without the voltage in the tensile stiffness tests. With the applied voltage, the mesh absorbs the stretchable layer, preventing it from being stretched and increasing the stiffness of the structure. An SSVS-AM unit is assembled with two anode meshes. With different voltages and a current of 20 mA applied to one and two anodes respectively, the variable-stiffness effect under 20% strain is shown in Figure 4b. It proves when the voltage increases, the tensile stiffness increases. For the test applying the voltage to one side of the mesh, the stiffness changes from 20 to 100 $N\,m^{-1}$. Compared to that, the result of applying a voltage to two sides of meshes shows that the stiffness changes from 20 to 820 $N\,m^{-1}$, and the stiffness can be continuously adjusted by voltage, and the stiffness gets small again when the voltage is removed. The results show that the effect of both meshes with applied voltage is much better than that of one mesh. Therefore, two meshes are used in all later studies. It can be seen in the result that the increase of the stiffness almost tends to level off when the applied voltage is over 700 V. The reason is that after the voltage has been increased to 700 V, the adsorption force is sufficient to ensure that the meshes attract the stretchable layer firmly with a high friction force, so increasing the voltage further will not increase the stiffness to a significantly higher value. The relationship between strain and stiffness at different voltages is also measured, as shown in Figure 4c. As the strain increases, the stiffness changes and the process can be divided into four stages: 1) In the first stage, the strain is under 20%, and the stiffness remains constant at the same voltage. The higher voltage applied, the bigger stiffness of the SSVS-AM. The reason for stiffness remaining constant is that with a very small strain (under 20%), the positions of the two meshes change very little. This ensures the structure maintains a high stiffness, and therefore it can be approximated as constant. 2) In the second stage, the strain is between 20% and 110%, the stiffness goes down approximately linearly as the strain is increased. In this stage, the stiffness of the SSVS-AM can be expressed as k in Equation (7), where k_U is the highest stiffness achieved with different voltages, β is the reduction in length of the stretchable layer being simultaneously attracted by two meshes. k_1 is the stiffness per unit length of the structure attracted by two meshes simultaneously, as expressed in Equation (8), where l_0 is the original length of the structure attracted by two meshes simultaneously. 3) In the third stage, the strain is between 110% and 160%. The SSVS-AM becomes a structure in which each end is attracted by a mesh, with only the stretched layer in the middle, where the stiffness

© 2023 The Authors. Advanced Intelligent Systems published by Wiley-VCH GmbH

26404567, 2023, 9, Downloaded from https://advanced.onlinelibrary.wiley.com/doi/10.1002/aisy.202300131 by Head Of Financial Services Bolland Library, Wiley Online Library on [14/10/2025]. See the Terms and Conditions (https://onlinelibrary.wiley.com/terms-and-conditions) on Wiley Online Library for rules of use; OA articles are governed by the applicable Creative Commons License

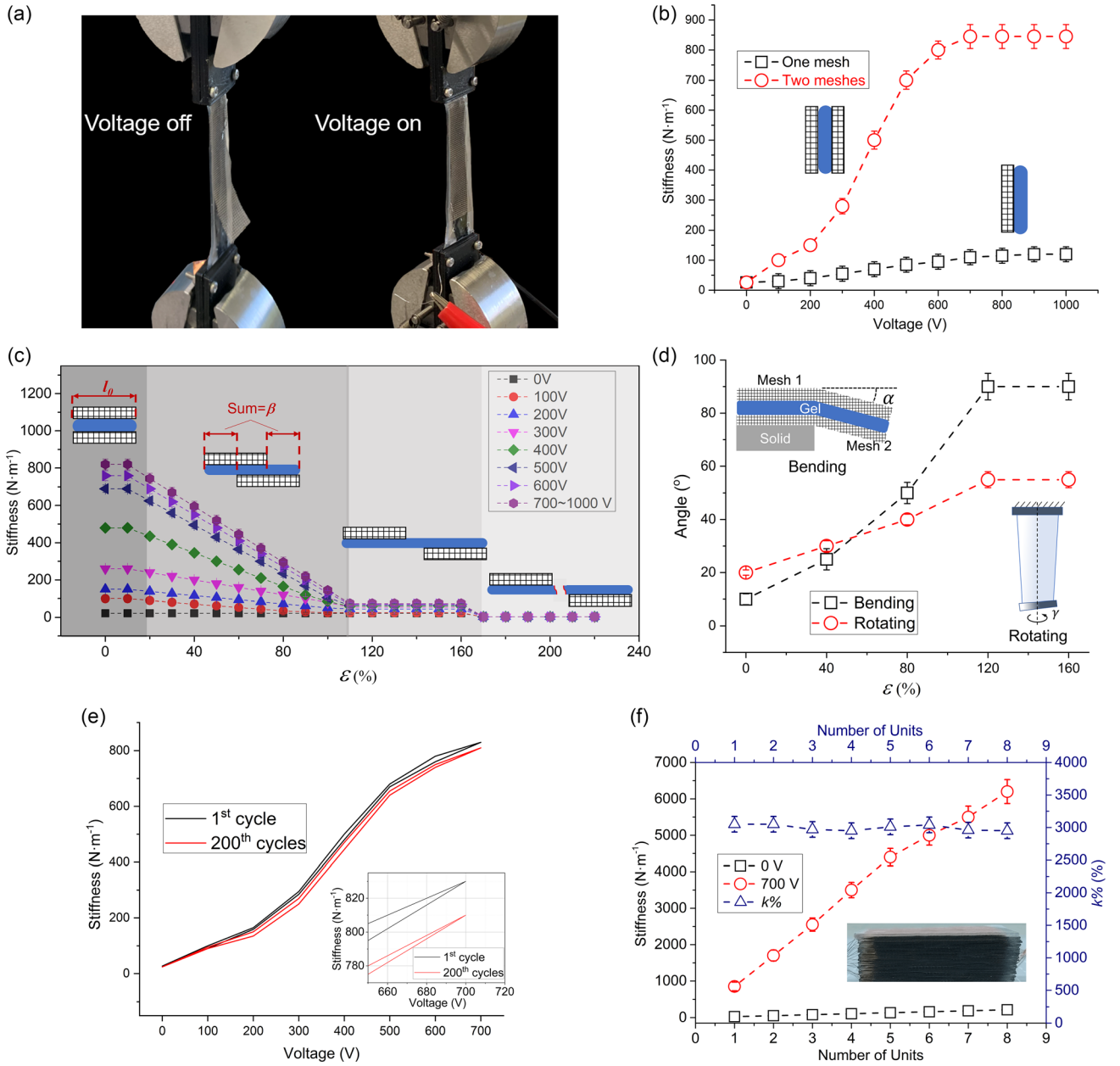

Figure 4. Tensile tests of the SSVS-AM. a) Instron 3342 is used to clamp both ends of the SSVS-AM for tensile stiffness testing (the stretching speed is 1 m s^{-1}), and the stiffness is obtained by measuring the tensile force and displacement. When the voltage is off, the mesh does not absorb the stretchable layer. When the voltage is on, the structure is harder to be stretched because the mesh absorbs the stretchable layer. b) Stiffness tests are carried out on SSVS-AMs with one and two meshes applied voltages from 0 to 1 kV, and the result shows that applying the voltage to two meshes will get a better variable-stiffness effect and that the stiffness will not increase when the voltage is above 700 V. c) Applying different voltages to the SSVS-AM, the stiffness of the structure changes as the stretching length varies. In the first stage (stretching up to 20%), the stretchable layer is absorbed and clamped by the two meshes in close proximity and the stiffness of the structure remains constant. In the second stage (stretching between 20% and 110%), as the stretching length increases, the two meshes become misaligned and the stiffness of the structure begins to decrease. In the third stage (stretching length between 110% and 160%), the two meshes are completely misaligned and the structural stiffness remains at a low level. In the fourth stage (stretching length over 160%), the stretchable layer is pulled off and the structural stiffness is zero. d) With various strains (stretching length between 0% and 160%) and 700 V applied, the maximum angles of bending and rotating are measured respectively. e) Variable-stiffness performance of the SSVS-AM for the 1st and the 200th voltage addition and reduction cycles. f) The tensile test of multiple SSVS-AM units in 0 and 700 V. The number of units and the increase in stiffness are approximately linear, and the *k*% remains almost constant.

© 2023 The Authors. Advanced Intelligent Systems published by Wiley-VCH GmbH

26404567, 2023, 9, Downloaded from https://advanced.onlinelibrary.wiley.com/doi/10.1002/aisy.202300131 by Head Of Financial Services Bolland Library, Wiley Online Library on [14/10/2025]. See the Terms and Conditions (https://onlinelibrary.wiley.com/terms-and-conditions) on Wiley Online Library for rules of use; OA articles are governed by the applicable Creative Commons License

26404567, 2023, 9, Downloaded from https://advanced.onlinelibrary.wiley.com/doi/10.1002/aisy.202300131 by Head Of Financial Services Bolland Library, Wiley Online Library on [14/10/2025]. See the Terms and Conditions (https://onlinelibrary.wiley.com/terms-and-conditions) on Wiley Online Library for rules of use; OA articles are governed by the applicable Creative Commons License

is low, nearly equal to the base stiffness of the stretched layer, below 100 N m^{-1}. 4) In the fourth stage, the strain is over 160%. The SSVS-AM is pulled off due to its modulus limitation, at which point the stiffness becomes zero.

To understand the bending and rotating performance of the SSVS-AM, two sets of experiments are performed as shown in Figure 4d. SSVS-AM is applied at 700 V and is subjected to different stretching rates (from 0% to 160%) to obtain the maximum bending angle (α) and the maximum rotating angle (γ). In other words, the meshes drop out of the gel, which is identified as a failure after exceeding the maximum angle. The biggest α occurs at a stretching rate of 160%, which is 90°, and the smallest α occurs at a stretching rate of 0%, which is 10°. The biggest γ occurs at a stretch rate of 160% and is 55°; the smallest γ occurs at a stretch rate of 0% and is 20°. This is because the modulus of the mesh is higher than the gel, and the bending and rotating resistances are stronger when the overlapping area of the mesh is smaller (the greater the stretching rate). As for the cycle life of the SSVS-AM, it is tested for up to 200 cycles of voltage addition and reduction, and the result is shown in Figure 4e. After 200 cycles, the variable-stiffness performance of the SSVS-AM remained almost constant (2.4% drop in stiffness at 700 V). The stiffness became less because of addition and adsorption tests, the surface of the gel is slightly worn during the stretching process, and the friction is slightly reduced after multiple voltage addition and adsorption tests. Since the surface of the wire mesh used in this work is polished, there is little wear on the gel and the variable-stiffness performance of the SSVS-AM is relatively stable. To investigate the effect of the number of units (one stretchable layer represents one unit) on the variable-stiffness performance, the test of multiple-layer systems is investigated, as is shown in Figure 4f. Since the units are added, the stiffness in 0 and 700 V increases linearly, and the rate of relative stiffness is relatively constant. Here, the rate of relative stiffness is defined as the percentage of the changed stiffness value compared to the initial stiffness value as shown in Equation (9).

$$k = k_U - \beta k_1 \tag{7}$$

$$k_1 = \frac{k_U}{l_0} \tag{8}$$

$$k\% = \frac{\Delta k}{k_0} \times 100\% \tag{9}$$

As expressed in Equation (9), k% is the rate of the relative stiffness, Δk is the changed stiffness, and k_0 is the initial stiffness.

2.4. Sensing of the SSVS-AM

As for the sensing performance (the sensitivity), the main factors are the components (CNT and Ecoflex 0-30) ratio and the thickness of the sensor layer. By mixing Ecoflex 00-30 with 10-20 nm multiwalled carbon nanotubes (MWCNT), the flexible resistive sensor has been successfully manufactured, as shown in Figure 2. To ensure the sensitivity and stretchability (it is known from the variable-stiffness performance that the sensor must meet the ability to stretch at least 160%), the concentration of MWCNT is chosen to be 2 wt%.[50,51] **Figure 5**c shows the scanning electron microscope image of the MWCNTs, which has an average diameter of 15 nm. After the length and width of the sensor are determined, its thickness is also an important factor in addition to the ratio of the sensor's components. The sensor and the PVC gel are combined together through the casting process to achieve the encapsulation of the sensor. The cross section of the structure is shown in Figure 2a. The results in Figure 5 show that when the structure is stretched by 140%, the three layers are still stuck together. Therefore, the combination of the two materials is functional.

Sensors (40 × 10 mm) of different CNT-Ecoflex layer thicknesses (20, 40, 60 μm) are tested in various stretched lengths (from 0 to 60 mm) using Instron E1000 (Figure 5a) and the result is shown in Figure 5b. The resistance (R) of the sensor with a 20 μm CNT-Ecoflex layer changes most obviously before and after being stretched (ΔL is the change of the sensor length), and the gauge factor (GF) (Equation (10)) value is bigger than the other two either GF_1 (the strain from 0 to 20 mm), or GF_2 (the strain from 20 to 40 mm), or GF_3 (the strain from 40 to 60 mm), as the results are shown in **Table 2**. Therefore, a sensor with a 20 μm MWCNT-Ecoflex layer is used as a cathode for the SSVS-AM. Figure 5d shows the trend in the resistance (or the relative resistance change) with increasing the length (or the strain), that is as the length increases, the resistance increases. To investigate the durability and hysteresis of the sensor, it is tested for hysteresis over 500 loading and unloading cycles, taking the results of the 1st, the 100th, and the 500th circle, respectively, as shown in Figure 5e. The difference among the three tests is not significant and shows a slight hysteresis in the resistance during the loading and unloading process, which may be related to the viscoelasticity of the silicone elastomer and PVC gel.

$$GF = (\Delta R/R_0)/\varepsilon = (\Delta R/R_0)/(\Delta L/L_0) \tag{10}$$

As expressed in Equation (10), ΔR is the change of the resistance, R_0 is the original resistance, ε is the strain, ΔL is the change of the sensor length, and L_0 is the original length of the sensor (40 mm).

Figure 5f illustrates the relationship among the stretch force (F), the strain (ε), and the relative resistance change ($\Delta R/R_0$) in various voltages from 0 to 700 V. Figure 5g shows that the SSVS-AM can sense different frequencies from 0 to 12 Hz (the common frequency range of human body vibrations).[52,53]

2.5. The Comparison Among Variable-Stiffness AMs

To evaluate the performance of variable stiffness of the SSVS-AM, we compare it with a list of currently available AMs in **Table 3**. These AMs can be classified as pneumatic, thermal, and electric according to the actuation energy. The pneumatic and thermal AMs have great performance in variable stiffness but have some delay in response. In contrast, the electric AMs have a fast response time, but the variable-stiffness performance still needs to be improved. The SSVS-AM, in contrast, balances these two relationships well, with both fast response speed and sufficient stiffness variation.

In addition to the SSVS-AM, there are mainly two other AMs based on the principle of electrostatic adsorption variable

© 2023 The Authors. Advanced Intelligent Systems published by Wiley-VCH GmbH

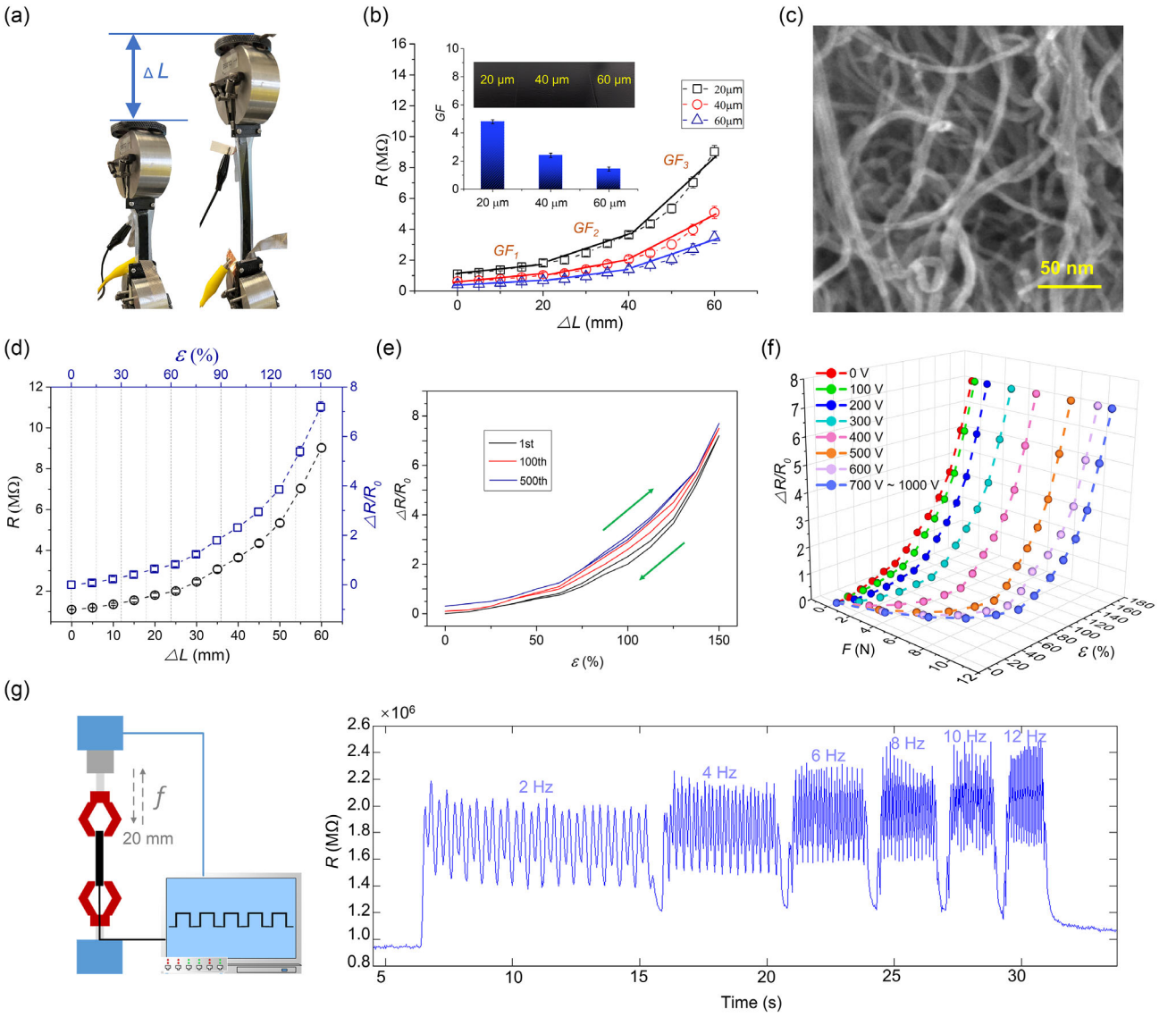

Figure 5. Tests of the SSVS-AM sensing performance. a) The testing system is based on Instron 3342 to measure the variation of the resistance of the sensor at different stretch lengths. b) The testing of three different thicknesses of sensors. The thinnest one is 20 μm thick, which has the biggest gauge factor (GF) and is the most sensitive. c) The scanning electron microscope image of the CNTs. d) The (relative) change in sensor resistance at 20 μm for different tensile lengths (strains). e) Hysteresis performance of the sensor (strain rate: 10% s^{-1}) at 160% stretch ratio for the 1st, the 100th, and the 500th loading and unloading cycles. f) The relationship among the stretch force (F), the strain (ε), and the relative resistance change ($\Delta R/R_0$) in various voltages from 0 to 700 V. g) The testing of the sensor's ability to sense vibrations using Instron E1000. With the stretched length of 20 mm, the sensor can measure the strain at a frequency of up to 12 Hz.

Table 2. GFs of the sensors in various thicknesses.

Thickness of the sensor [μm]	GF_1	GF_2	GF_3
20	2.2	3.7	4.1
40	0.9	1.5	2.2
60	0.5	0.9	1.3

stiffness, as shown in **Figure 6**a, one is the fringe electric-field-enabled variable stiffness (FEVS) AM, and the other is the electrostatic layer jamming (ELJ) laminates. The FEVS AM uses the electroadhesion (EA) technology based on the fringe electric field. The variable-stiffness principle for the FEVS is that when the EA pads are actuated, they will polarize the interlayer, and attract it to increase the friction between each other so that the structural stiffness increases. The principle of the ELJ is that the electrode layers are applied with opposite voltages, and an electric field goes through the interlayer. When the two electrode layers attract each other, the interlayer will be compressed, which leads to an increase in the frictional force, and therefore the stiffness of the whole structure increases. Using the same area

© 2023 The Authors. Advanced Intelligent Systems published by Wiley-VCH GmbH

26404567, 2023, 9, Downloaded from https://advanced.onlinelibrary.wiley.com/doi/10.1002/aisy.202300131 by Head Of Financial Services Bolland Library, Wiley Online Library on [14/10/2025]. See the Terms and Conditions (https://onlinelibrary.wiley.com/terms-and-conditions) on Wiley Online Library for rules of use; OA articles are governed by the applicable Creative Commons License

Table 3. The comparison of different types of variable-stiffness artificial muscles.

Artificial muscle	Actuation energy	Responsive time	Maximum k% of one unit
Soft jamming brake and artificial muscle[55]	Pneumatic	≈ 200 ms	≈ 3500
Variable-stiffness linear actuator[56]	Pneumatic	≈ 500 ms	≈ 2130
Variable-stiffness dielectric elastomer actuator[57]	Thermal	≈ 30 s	≈ 10^6
Twisted and coiled polymer actuator with strain self-sensing ability[34]	Thermal	≈ 50 s	≈ 40
Twisted rubber artificial muscle[58]	Thermal	≈ 10 s	≈ 90
Fringe-electric-field-enabled variable-stiffness (FEVS) artificial muscle[23]	Electric	< 10 ms	≈ 175
Electrostatic layer jamming (ELJ)[22]	Electric	< 10 ms	≈ 59
SSVS-AM	Electric	< 10 ms	≈ 3000

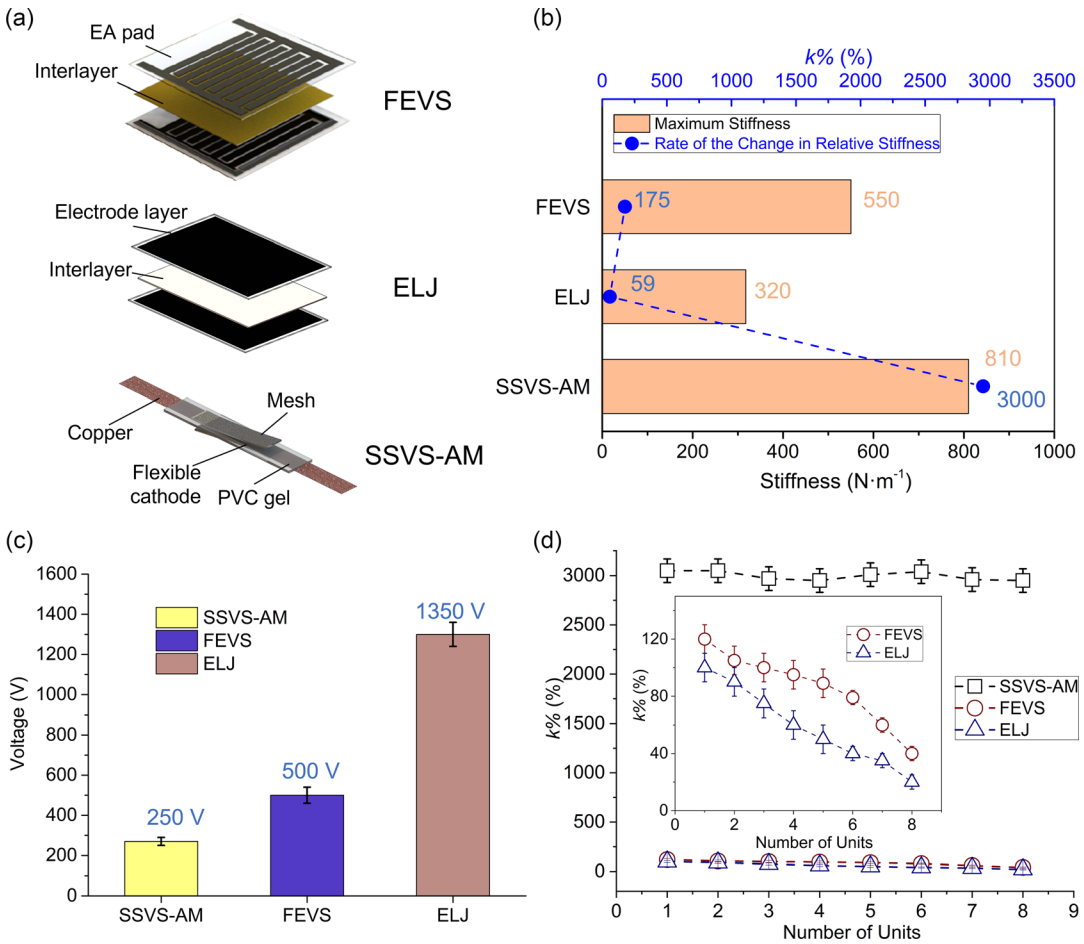

Figure 6. The comparisons of three variable-stiffness AMs based on the electrostatic adsorption technology. a) The three similar AMs: field-enabled variable-stiffness (FEVS),[23] electrostatic layer jamming (ELJ), and SSVS-AM. b) The maximum stiffness and the corresponding k% of three AMs in the size of 40 × 10 mm, and it shows the SSVS-AM can reach the biggest stiffness and the k%. c) To get the same stiffness of 500 N m^{-1}, the different voltages are applied on the three AMs. The SSVS-AM uses the lowest voltage with only 250 V, the FEVS uses 500 V, and the ELJ uses 1350 V. d) The relationship between the number of units and the k% of the three AMs.

dimensions (40 × 10 mm), the SSVS-AM is compared with FEVS and ELJ in terms of variable-stiffness performance. As shown in Figure 6b, the FEVS, the ELJ, and the SSVS-AM can reach the maximum stiffness and the corresponding k% as 550 N m^{-1} and 175%, 320 N m^{-1} and 59%, 810 N m^{-1} and 3000%, respectively. Therefore, the SSVS-AM has a significantly improved capacity to generate a variable stiffness. To get the same stiffness of 500 N m^{-1}, the SSVS-AM uses the lowest voltage of only 250 V, while the FEVS uses 500 V, and the ELJ uses 1350 V, as shown in Figure 6c. Figure 6d shows the relationship between the number of units and the k% of the three AMs. As the number of units increases from 1 to 8, the k% remains

© 2023 The Authors. Advanced Intelligent Systems published by Wiley-VCH GmbH

26404567, 2023, 9, Downloaded from https://advanced.onlinelibrary.wiley.com/doi/10.1002/aisy.202300131 by Head Of Financial Services Bolland Library, Wiley Online Library on [14/10/2025]. See the Terms and Conditions (https://onlinelibrary.wiley.com/terms-and-conditions) on Wiley Online Library for rules of use; OA articles are governed by the applicable Creative Commons License

constant (about 3000%) for the SSVS-AM, and for the FEVS and the ELJ, the k% decreases from 120% to 50%, and from 100% to 25%, respectively. The anode mesh (actuation layer) of the SSVS-AM acts as an independent layer when it is without the voltage and it does not change the original modulus of the structure as the number of units increases. In contrast, the other two AMs have actuation layers that are not independent and increase the base modulus of the structure as the number of units increases, the k% therefore decreases.

3. Conclusions

In this article, a novel SSVS AM is proposed referencing the biological smooth muscle contraction. The results showed that the SSVS-AM, which integrated actuation with the sensing function, processes over 10 times improved capacity to adjust stiffness along the stretching direction with voltages (0–700 V), which is lower compared with the existing electric variable-stiffness AMs (the fringe electric FEVS AM and the ELJ laminates). Moreover, it is also capable of fast response (under 100 ms) based on the signal detected by its sensing function. The integrated sensing-actuation function provides a promising solution to make the design and control of soft robots simpler than the traditional ways which use separate sensors and actuators. Future work will explore better combinations of the PVC gel layer and the CNT-Ecoflex layer to further improve the sensing performance. The SSVS-AM has good prospects for application in the field of wearable rehabilitation robots, where its ability to monitor deformation and provide stiffness will come into play. In addition, the low output power (although the voltage is several hundred volts, the current is only a few microamps) ensures safe wear.

4. Experimental Section

Materials: The Ecoflex 00-30 was purchased from Smooth-On, Inc. The mesh was purchased from Electronic Materials Ltd. UK. DBA, tetrahydrofuran (THF), and isopropanol (IPA) are purchased from Sigma–Aldrich, USA. The copper tape was purchased from RS Components, UK. The MWCNTs with 98% purity and 10–25 μm length were supplied by IoLiTec-Ionic Liquid Technologies GmbH. The PVC powder was purchased from Scientific Polymer Products, Inc.

Preparation of PVC Gel Solution: The PVC powder was mixed with DBA and THF, and the weight ratio was

$$(\mathrm{mPVC}:\mathrm{mDBA}):\mathrm{mTHF} = (1:4):3 \tag{11}$$

THF and DBA were first stirred in a sealed bottle for 5 min with a magnetic stirrer (800 r min^{-1}), and then the PVC powders were added. Without heating, the three materials were stirred for at least 12 h.

Preparation of CNT-Ecoflex 00-30 Solution: The 1 L IPA and 0.5 g CNT were ultrasonically dispersed for 2 h. The same weight A and B components of the Ecoflex 00-30 were added to the dispersed CNT solution, and the mass of the Ecoflex and the CNT were defined as mEcoflex and mCNT, respectively. The mass ratio was

$$\mathrm{mEcoflex}:\mathrm{mCNT} = 49:1 \tag{12}$$

They were heated to 60 °C by a magnetic mixer and stirred (500 r min^{-1}) for about 10 h.

Casting: The Elcometer 4340 was used to cast different solutions, whose resolution of the thickness was 10 μm. Air bubbles needed to be removed from the solution by evacuation or standing before casting. The moving speed of the film applicator coater for the casting was 2 m min^{-1}, and the heating temperatures were 40 °C for the PVC gel layer and 80 °C for CNT-Ecoflex 00-30 layer. Because the PVC gel solution would volatilize THF after casting, it was currently possible to achieve a minimum of 30 μm for PVC gel based on the level of the process. And for the CNT-Ecoflex layer, the minimum thickness was 20 μm.

Variable Stiffness and Sensing Tests: Instron 3342 (Instron, UK) was used to stretch the SSVS-AM, it could record the length changing precisely (0.001 mm) and the force (0–20 N). The Arduino Uno board (Arduino. CC) was used to output the control voltage from 0 to 5 V, and it was also used to collect the resistance changes produced by the SSVS-AM. The amplifier (XP Power Q10-5 DC, from XP Power, UK) was connected to the Arduino Uno board to transfer low voltage (0–5 V) to high voltage (0–1000 V), then output it to the SSVS-AM for variable stiffness. MATLAB 2021 was used to acquire and plot signal images. Instron E1000 (Instron, UK) was used to generate the simple harmonic displacement to verify the SSVS-AM that can detect different displacements in various frequencies.

D Printing for Attachment of the Testing: Ultimaker S3 (Ultimaker, USA) was used to print some attachments for testing, for instance, the clamps. The material was polylactic acid, which was purchased from RS Components, UK.

Supporting Information

Supporting Information is available from the Wiley Online Library or from the author.

Acknowledgements

This work is partially supported by Engineering and Physical Sciences Research Council (EPSRC), National Centre for Nuclear Robotics (NCNR) EP/R02572X/1; Royal Society, International Exchanges Cost Share award EC\NSFC\211324, China Scholarship Council (CSC). The authors thank Thomas Mack's assistance with reviewing the writing.

Conflict of Interest

The authors declare no conflict of interest.

Data Availability Statement

The data that support the findings of this study are available from the corresponding author upon reasonable request.

Keywords

artificial muscles, self-sensing, soft sensors, variable stiffness

Received: March 13, 2023
Revised: May 17, 2023
Published online: July 8, 2023

[1] Y. Lin, G. Yang, Y. Liang, C. Zhang, W. Wang, D. Qian, H. Yang, J. Zou, *Adv. Funct. Mater.* **2020**, *30*, 2000349.
[2] J. Zhou, Y. Chen, Y. Hu, Z. Wang, Y. Li, G. Gu, Y. Liu, *Soft robotics* **2020**, *7*, 743.
[3] Y. Zhong, R. Du, L. Wu, H. Yu, in *IEEE Inter. Conf. on Robotics and Automation (ICRA)*, IEEE, Piscataway, NJ **2020**, pp. 2939–2945.

© 2023 The Authors. Advanced Intelligent Systems published by Wiley-VCH GmbH

26404567, 2023, 9, Downloaded from https://advanced.onlinelibrary.wiley.com/doi/10.1002/aisy.202300131 by Head Of Financial Services Bolland Library, Wiley Online Library on [14/10/2025]. See the Terms and Conditions (https://onlinelibrary.wiley.com/terms-and-conditions) on Wiley Online Library for rules of use; OA articles are governed by the applicable Creative Commons License

[4] D. Rus, *Nature* **2015**, *521*, 467.
[5] J. Wang, D. Gao, P. S. Lee, *Adv. Mater.* **2021**, *33*, 2003088.
[6] J. Rubenson, G. S. Sawicki, *Sci. Robot.* **2022**, *7*, eabo2147.
[7] D. Wisth, M. Camurri, M. Fallon, *IEEE Trans. Robot.* **2022**.
[8] G. Li, X. Chen, F. Zhou, Y. Liang, Y. Xiao, X. Cao, Z. Zhang, M. Zhang, B. Wu, S. Yin, Y. Xu, H. Fan, Z. Chen, W. Song, W. Yang, B. Pan, J. Hou, W. Zou, S. He, X. Yang, G. Mao, Z. Jia, H. Zhou, T. Li, S. Qu, Z. Xu, Z. Huang, Y. Luo, T. Xie, J. Gu, et al., *Nature* **2021**, *591*, 66.
[9] I. Must, E. Sinibaldi, B. Mazzolai, *Nat. Commun.* **2019**, *10*, 344.
[10] Y. Wang, P. Zhang, H. Huang, J. Zhu, *Soft Robot.* **2022**.
[11] C. Tang, B. Du, S. Jiang, Q. Shao, X. Dong, X. J. Liu, H. Zhao, *Sci. Robot.* **2022**, *7*, eabm8597.
[12] J. Yan, Z. Xu, P. Shi, J. Zhao, *Soft Robot.* **2022**, *9*, 399.
[13] J. Lussi, M. Mattmann, S. Sevim, F. Grigis, C. De Marco, C. Chautems, S. Pané, J. Puigmartí-Luis, Q. Boehler, B. J. Nelson, *Adv. Sci.* **2021**, *8*, 2101290.
[14] I. Vitanov, I. Farkhatdinov, B. Denoun, F. Palermo, A. Otaran, J. Brown, B. Omarali, T. Abrar, M. Hansard, C. Oh, S. Poslad, C. Liu, H. Godaba, K. Zhang, L. Jamone, K. Althoefer, *Robotics* **2021**, *10*, 112.
[15] P. H. Nguyen, W. Zhang, *Sci. Rep.* **2020**, *10*, 9638.
[16] Z. Jiang, K. Zhang, in *IEEE Int. Conf. on Robotics and Automation (ICRA)*, IEEE, Piscataway, NJ **2021**, pp. 9318–9324.
[17] C. Yang, W. Wu, X. Wu, J. Zhou, Z. Tu, M. Lin, S. Zhang, *Industr. Robot* **2022**, *49*, 1190.
[18] H. Wang, Z. Chen, S. Zuo, *Soft Robot.* **2022**, *9*, 577.
[19] D. Zappetti, S. H. Jeong, J. Shintake, D. Floreano, *Soft Robot.* **2020**, *7* 362.
[20] S. Akbari, A. H. Sakhaei, S. Panjwani, K. Kowsari, Q. Ge, *Sens. Actuators A: Phys.* **2021**, *321*, 112598.
[21] R. Hinchet, H. Shea, *Adv. Mater. Technol.* **2020**, *5*, 1900895.
[22] T. Wang, J. Zhang, Y. Li, J. Hong, M. Y. Wang, *IEEE/ASME Trans. Mechatron.* **2019**, *24*, 424.
[23] C. Liu, B. Li, Z. Li, C. Cao, X. Gao, K. Zhang, H. Chen, *Soft Matter* **2021**, *17*, 6697.
[24] L. Chang, D. Wang, Z. Huang, C. Wang, J. Torop, B. Li, Y. Wang, Y. Hu, A. Aabloo, *Adv. Funct. Mater.* **2022**, 2212341.
[25] Y. Zhang, J. Yang, X. Hou, G. Li, L. Wang, N. Bai, M. Cai, L. Zhao, Y. Wang, J. Zhang, K. Chen, X. Wu, C. Yang, Y. Dai, Z. Zhang, C. F. Guo, *Nat. Commun.* **2022**, *13*, 1317.
[26] J. Zhao, J. Fang, S. Wang, K. Wang, C. Liu, T. Han, *Sensors* **2021**, *21*, 6777.
[27] T. Jin, Z. Sun, L. Li, Q. Zhang, M. Zhu, Z. Zhang, G. Yuan, T. Chen, Y. Tian, X. Hou, C. Lee, *Nat. Commun.* **2020**, *11*, 5381.
[28] K. B. Justus, T. Hellebrekers, D. D. Lewis, A. Wood, C. Ingham, C. Majidi, P. R. Leduc, C. Tan, *Sci. Robot.* **2019**, *4*, eaax0765.
[29] Z. Shen, Z. Zhang, N. Zhang, J. Li, P. Zhou, F. Hu, Y. Rong, B. Lu, G. Gu, *Adv. Mater.* **2022**, 2203650.
[30] M. Y. Liu, C. Z. Hang, X. Y. Wu, L. Y. Zhu, X. H. Wen, Y. Wang, X. F. Zhao, H. L. Lu, *Nanotechnology* **2022**, *33*, 255501.
[31] A. Tonazzini, J. Shintake, C. Rognon, V. Ramachandran, S. Mintchev, D. Floreano, in *IEEE Int. Conf. on Soft Robotics (RoboSoft)*, IEEE, Piscataway, NJ **2018**, pp. 485–490.
[32] M. Jin, M. Jin, L. Zhang, R. Yang, *IEEE Sens. J.* **2021**, *21*, 27076.
[33] Z. Liu, R. Zhang, Y. Xiao, J. Li, W. Chang, D. Qian, Z. Liu, *Mater. Horizons* **2021**, *8* 1783.
[34] P. Zhao, B. Xu, Y. Zhang, B. Li, H. Chen, *ACS Appl. Mater. Interfaces* **2020**, *12*, 15716.
[35] D. Zhang, X. Wang, Y. Wu, H. Song, Z. Ma, X. Zhang, X. Yang, R. Xing, Y. Li, J. Yang, *Adv. Mater. Technol.* **2021**, *6*, 2100106.
[36] Z. Wang, W. Lu, F. An, M. Song, D. Ponge, D. Raabe, Z. Li, *Nat. Commun.* **2022**, *13*, 3598.
[37] Z. Chen, Z. Ma, J. Tang, Y. Xiao, J. Mao, Y. Cai, J. Zhao, X. Gao, T. Li, Y. Luo, *Mater. Horizons* **2021**, *8*, 2834.
[38] C. Demolder, A. Molina, *Biosens. Bioelectron.* **2021**, *190*, 113443.
[39] A. Zahedi, B. Zhang, A. Yi, D. Zhang, *Soft Robot.* **2021**, *8*, 432.
[40] C. Hernández-Santos, Y. A. Davizón, A. R. Said, R. Soto, L. Felix-Herrán, A. Vargas-Martínez, *Appl. Sci.* **2021**, *11*, 4145.
[41] M. A. Vélez-Guerrero, M. Callejas-Cuervo, S. Mazzoleni, *Sensors* **2021**, *21*, 2146.
[42] Y. Li, M. Hashimoto, *Sens. Actuators A: Phys.* **2015**, *233*, 246.
[43] C. Wang, R. Li, Z. Zhu, J. H. Wu, F. Ma, *Eng. Struct.* **2022**, *269*, 114777.
[44] Y. Li, M. Guo, Y. Li, *J. Mater. Chem. C* **2019**, *7*, 12991.
[45] I. Morano, G. X. Chai, L. G. Baltas, V. Lamounier-Zepter, G. Lutsch, M. Kott, H. Haase, M. Bader, *Nat. Cell Biol.* **2000**, *2*, 371.
[46] A. Horowitz, C. B. Menice, R. Laporte, K. G. Morgan, *Physiol. Rev.* **1996**, *76*, 967.
[47] R. C. Webb, *Adv. Physiol. Educ.* **2003**, *27*, 201.
[48] K. Asaka, M. Hashimoto, *Sens. Actuators B: Chem.* **2018**, *273*, 1246.
[49] Y. Li, Y. Li, M. Hashimoto, *Sens. Actuators B: Chem.* **2019**, *282*, 482.
[50] Z. Tang, S. Jia, F. Wang, C. Bian, Y. Chen, Y. Wang, B. Li, *ACS Appl. Mater. Interfaces* **2018**, *10*, 6624.
[51] P. Ciselli, L. Lu, J. J. Busfield, T. Peijs, *e-Polymers* **2010**, *10*, 014.
[52] J. Benito-Leon, E. D. Louis, *Nat. Clin. Pract. Neurol.* **2006**, *2*, 666.
[53] T. Novak, K. M. Newell, *Neurosci. Lett.* **2017**, *641*, 87.
[54] Art S. M., Locomotor System Archives. Servier Medical Art, **2022**, p. 1.
[55] B. H. Do, I. Choi, S. Follmer, *IEEE/ASME Trans. Mechatron.* **2022**, *27*, 5529.
[56] L. Arleo, L. Lorenzon, M. Cianchetti, *IEEE Trans. Robot.* **2023**.
[57] J. Shintake, B. Schubert, S. Rosset, H. Shea, D. Floreano, in *IEEE/RSJ Int. Conf. on Intelligent Robots and Systems (IROS)*, IEEE, Piscataway, NJ **2015**, pp. 1097–1102.
[58] T. Helps, M. Taghavi, S. Wang, J. Rossiter, *Soft Robot.* **2020**, *7*, 386.

© 2023 The Authors. Advanced Intelligent Systems published by Wiley-VCH GmbH

26404567, 2023, 9, Downloaded from https://advanced.onlinelibrary.wiley.com/doi/10.1002/aisy.202300131 by Head Of Financial Services Bolland Library, Wiley Online Library on [14/10/2025]. See the Terms and Conditions (https://onlinelibrary.wiley.com/terms-and-conditions) on Wiley Online Library for rules of use; OA articles are governed by the applicable Creative Commons License